Quantum magneto-electrodynamics of electrons embedded in a photon cavity

2012 New J. Phys. 14 013036

(http://iopscience.iop.org/1367-2630/14/1/013036)

New Journal of Physics
The open-access journal for physics

Quantum magneto-electrodynamics of electrons embedded in a photon cavity

Olafur Jonasson[1], Chi-Shung Tang[2], Hsi-Sheng Goan[3,4], Andrei Manolescu[5] and Vidar Gudmundsson[1,6]

[1] Science Institute, University of Iceland, Dunhaga 3, IS-107 Reykjavik, Iceland
[2] Department of Mechanical Engineering, National United University, 1, Lienda, Miaoli 36003, Taiwan
[3] Department of Physics and Center for Theoretical Sciences, National Taiwan University, Taipei 10617, Taiwan
[4] Center for Quantum Science and Engineering, National Taiwan University, Taipei 10617, Taiwan
[5] Reykjavik University, School of Science and Engineering, Menntavegur 1, IS-101 Reykjavik, Iceland
E-mail: olafur.jonasson@gmail.com, vidar@hi.is and cstang@nuu.edu.tw

New Journal of Physics **14** (2012) 013036 (15pp)
Received 21 September 2011
Published 19 January 2012
Online at http://www.njp.org/
doi:10.1088/1367-2630/14/1/013036

Abstract. We investigate the coupling between a quantized electromagnetic field in a cavity resonator and a Coulomb interacting electronic system in a nanostructure in an external magnetic field. The effects caused by the geometry of the electronic system and the polarization of the electromagnetic field are explicitly taken into account. Our numerical results demonstrate that the two-level system approximation and the Jaynes–Cummings model remain valid in the weak electron–photon coupling regime, while the quadratic vector potential in the diamagnetic part of the charge current leads to significant correction to the energy spectrum in the strong coupling regime. Furthermore, we find that coupling to a strong cavity photon mode polarizes the charge distribution of the system, requiring a large basis of single-electron eigenstates to be included in the model.

[6] Author to whom any correspondence should be addressed.

Contents

1. Introduction

Over the last decade, there has been increasing interest in systems capable of generating quantized fields containing a preset number of photons. Manipulation of the state of scalable light–matter coupled quantum systems is one of the key issues in their implementation for optomechanical systems [1, 2] or quantum information processing devices [3, 4]. However, to search for clear evidence of light–matter coupling nonlinearity is still a challenge. To this end, one has to reach a strong light–matter coupling regime for optically driven systems in high-quality micro-cavities [5, 6] and demonstrate its single-photon characteristics [7, 8]. Flexible experimental design of circuit quantum electrodynamics offers great potential for practical device applications to explore strong light–matter coupling at microwave frequencies [9–13].

To describe the interaction between matter and the photons of a quantized electromagnetic field, the Jaynes–Cummings (JC) model is often applied [14]. The JC model describes the interaction between a two-level system (TLS) and a single-field mode. It is a fundamental model in quantum optics and quantum information science [15]. For a TLS with energy level spacing ΔE, coupled with strength $\mathcal{E}_{\rm JC}$ to a resonator with photon energy $\hbar\omega$, the JC model is valid when both the detuning $\delta = |\hbar\omega - \Delta E|$ is sufficiently small and the light–matter coupling strength is much smaller than the photon energy ($\mathcal{E}_{\rm JC} \ll \hbar\omega$). The dynamics can then be obtained by the JC model [16] and the energy spectrum can be solved exactly if the rotating wave approximation (RWA) is applied [17].

Single modes of the electromagnetic field can be treated as the population of a field oscillator with different Fock states (states with a certain number of photons). It was discovered that a three-level problem, called the coupled-channel cavity quantum electrodynamics model [18], can be exactly transformed to a two-level one for arbitrary detuning [19], in which the eigenstates of energy and orbital angular momentum can be explicitly expressed in terms of the Fock states.

More recently, the utilization of the giant dipole moments of intersubband transitions in quantum wells [20, 21] has enabled researchers to reach the ultrastrong light–matter coupling regime [22–24]. In this regime, the JC model is not applicable and the coupling mechanism has to be explored beyond the JC model [25–27]. Despite the above-mentioned experiments, a study of the coupling between electrons and cavity photons with a specified nanostructure geometry in a perpendicular magnetic field is still lacking.

In this paper, we investigate the interplay of the dynamics of correlated electrons in a nanostructure to the quantum field of a rectangular cavity resonator subject to an external magnetic field. By performing numerical computations, we demonstrate how the electron–photon coupling influences an electronic system embedded in a quantized photon field.

The TLS approximation and the JC model will be examined in both the weak and the strong coupling regimes as well as the effects of the diamagnetic part of the charge current in the electron–photon interaction term, which the JC model lacks.

2. Model and theory

The system under investigation is a two-dimensional (2D) electronic nanostructure exposed to a quantized electromagnetic field of a cavity resonator and a static (classical) external magnetic field at a low temperature. The electron–photon coupled system can be described by the many-body Hamiltonian

$$H = H_{\mathrm{e}} + H_{\mathrm{EM}} + H_{\mathrm{e-EM}}, \tag{1}$$

where the first term describes the electronic system including the magnetic-field modified kinetic term H_{e}^{0} and a Coulomb interaction term H_{Coul}, namely

$$H_{\mathrm{e}} = H_{\mathrm{e}}^{0} + H_{\mathrm{Coul}}. \tag{2}$$

The second term H_{EM} in equation (1) represents the electromagnetic field in a cavity resonator and the third term $H_{\mathrm{e-EM}}$ contains the coupling between the electronic system and the quantized electromagnetic field.

The electronic nanostructure is assumed to be fabricated by split-gate configuration in the y-direction, forming a parabolic confinement with the characteristic frequency Ω_0 on top of a semiconductor heterostructure. The ends of the nanostructure in the x-direction at $x = \pm L_x/2$ are etched, forming a hard-wall confinement of length L_x. Thereby, a closed electronic narrow constriction is created in the 2D electron gas. The external classical magnetic field is given by $\mathbf{B} = B\hat{\mathbf{z}}$ with a vector potential $\mathbf{A}_{\mathrm{ext}} = (-By, 0)$. Hence, H_{e}^{0} can be expressed in the second quantization as

$$H_{\mathrm{e}}^{0} = \int \mathrm{d}\mathbf{r}\psi^{\dagger}\left\{\frac{\pi^{2}}{2m^{*}} + \frac{1}{2}m^{*}\Omega_{0}^{2}y^{2}\right\}\psi, \tag{3}$$

where $\boldsymbol{\pi} = \mathbf{p} + e\mathbf{A}_{\mathrm{ext}}/c$ is the mechanical momentum, m^{*} is the effective electron mass and

$$\psi = \sum_{i}\psi_{i}(\mathbf{r})d_{i}, \quad \psi^{\dagger} = \sum_{i}\psi_{i}^{*}(\mathbf{r})d_{i}^{\dagger} \tag{4}$$

are fermionic field operators, with d_i being the annihilation and $d_i^{\dagger}$ the creation operator for an electron in the single electron state $|i\rangle$ corresponding to ψ_i. Throughout this paper we use Latin indices to label single-electron states (SESs) as well as Hilbert state vectors and Greek subscripts to label many-electron Fock states (MESs). Rationalized Gaussian units are used exclusively and e denotes the positive elementary charge. In equation (4), $\psi_i(\mathbf{r})$ can be any complete orthonormal set of functions with the correct boundary conditions. However, if we use the SESs of H_{e}^{0} as a basis, H_{e}^{0} is diagonal and simplifies to

$$H_{\mathrm{e}}^{0} = \sum_{i}E_{i}d_{i}^{\dagger}d_{i}, \tag{5}$$

where E_i is the energy of the SES i, associated with the eigenfunction $\psi_i(\mathbf{r})$. The SESs are computed numerically in a functional basis using a straightforward diagonalization method.

We can write the Coulomb interaction term in the second quantized form

$$H_{\rm Coul} = \frac{1}{2}\sum_{ijrs}\langle ij|V_{\rm Coul}|rs\rangle d_i^\dagger d_j^\dagger d_s d_r, \tag{6}$$

where the Coulomb interaction potential can be written as

$$V_{\rm Coul}(\mathbf{r},\mathbf{r}') = \frac{e^2/\kappa}{|\mathbf{r}-\mathbf{r}'|+\eta^2}, \tag{7}$$

with κ denoting the relative dielectric constant of the material and η an infinitesimal convergence parameter. The Coulomb matrix elements in equation (6) are thus expanded in the basis of the SESs involving the integration with respect to the observing location $\mathbf{r}$

$$\langle ij|V_{\rm Coul}|rs\rangle = \int {\rm d}\mathbf{r}\ \psi_i^*(\mathbf{r})\mathcal{I}_{jr}(\mathbf{r})\psi_s(\mathbf{r}) \tag{8}$$

and the integration with respect to the source location $\mathbf{r}'$

$$\mathcal{I}_{jr}(\mathbf{r}) = \int {\rm d}\mathbf{r}'\psi_j^*(\mathbf{r}')V_{\rm Coul}(\mathbf{r},\mathbf{r}')\psi_r(\mathbf{r}'). \tag{9}$$

We use the SESs to construct MESs $|\mu\rangle$ which obey $H_{\rm e}^0|\mu\rangle = E_\mu|\mu\rangle$, and employ an exact numerical diagonalization method to obtain, in the (noninteracting) basis $\{|\mu\rangle\}$, the Coulomb interacting eigenvectors $|\mu)$ which satisfy $(H_{\rm e}^0 + H_{\rm Coul})|\mu) = \tilde{E}_\mu|\mu)$. We write the Coulomb interacting eigenvectors in terms of a unitary transformation ([29, 30] and references therein)

$$|\mu) = \sum_\nu \mathcal{V}_{\mu\nu}|\nu\rangle, \tag{10}$$

which is obtained in the diagonalization process. Then, in the new interacting MES basis $\{|\mu)\}$, we can rewrite the full electron Hamiltonian as

$$H_{\rm e} = \sum_\mu |\mu)\tilde{E}_\mu(\mu|. \tag{11}$$

The cavity electromagnetic field is described by the quantized vector potential $\mathbf{A}$ in the radiation (Coulomb) gauge. The free field Hamiltonian is simply

$$H_{\rm EM} = \hbar\omega a^\dagger a, \tag{12}$$

where ω is the frequency of the resonant cavity mode and $a^\dagger$ and a are the creation and annihilation operators for photons. The last term in equation (1) describing the interaction between the electrons and the quantized electromagnetic field is given by

$$H_{\rm e-EM} = -\frac{1}{c}\int {\rm d}\mathbf{r}\,\mathbf{j}_{\rm e}\cdot\mathbf{A} - \frac{e}{2m^*c^2}\int {\rm d}\mathbf{r}\,\rho_{\rm e}A^2, \tag{13}$$

in which the charge current density is defined by

$$\mathbf{j}_{\rm e} = -\frac{e}{2m^*}\left\{\psi^\dagger(\boldsymbol{\pi}\psi) + (\boldsymbol{\pi}^*\psi^\dagger)\psi\right\}, \tag{14}$$

and the charge density $\rho_{\rm e} = -e\psi^\dagger\psi$. In this paper, we will show that the A^2 term in equation (13) significantly affects dynamical features in the strong electron–photon coupling regime. The electronic nanostructure is placed in a rectangular cavity forming an electromagnetic oscillator with hard-wall boundaries at $-a_{\rm c}/2 < x, y < a_{\rm c}/2$ and $-d_{\rm c}/2 < z < d_{\rm c}/2$ with cavity volume $V_{\rm c} = a_{\rm c}^2 d_{\rm c}$. The proposed electromagnetic oscillator is a single

planar rectangular cavity with mutually locked dual anti-phase outputs, in which the electronic nanostructure is oriented in the $z = 0$ plane with the center at $(x, y) = (0, 0)$. In the following, we will consider only transverse electric (TE) modes ($E_z = 0$), where the electric field $\mathbf{E}$ is perpendicular to the direction of propagation. The cavity supplies a monochromatic wave stabilized in the TE_{011} mode with longitudinally polarized electric field along the x-direction or in the TE_{101} mode with transversely polarized electric field along the y-direction. In the Coulomb gauge, the vector potential of the electromagnetic field takes the form

$$\mathbf{A}(\mathbf{r}) = \begin{pmatrix} \hat{\mathbf{e}}_x \\ \hat{\mathbf{e}}_y \end{pmatrix} \mathcal{A} \begin{bmatrix} \cos\left(\frac{\pi x}{a_c}\right) \\ \cos\left(\frac{\pi y}{a_c}\right) \end{bmatrix} \cos\left(\frac{\pi z}{d_c}\right) \left(a + a^\dagger\right), \tag{15}$$

with the upper component denoting the TE_{011} mode and the lower one representing the TE_{101} mode. The Cartesian unit vectors are $\hat{\mathbf{e}}_x$ and $\hat{\mathbf{e}}_y$.

We assume that the size of the cavity is much larger than that of the nanostructure, that is, $L_x \ll a_c, d_c$. Utilizing this condition we can approximate the cosines in equation (15) by unity and take $\mathbf{A}$ outside the integrals in equation (13) and obtain

$$H_{e-EM} = \mathcal{E}_c \sum_{i,j} d_i^\dagger d_j \, g_{ij} \left(a + a^\dagger\right) + \frac{\mathcal{E}_c^2}{\hbar \Omega_w} \mathcal{N}_e \left[\left(a^\dagger a + \frac{1}{2} \right) + \frac{1}{2} \left(a^\dagger a^\dagger + aa \right) \right], \tag{16}$$

where $\Omega_w = \sqrt{\Omega_0^2 + \omega_c^2}$ is the effective confinement frequency, $\omega_c = eB/(m^* c)$ the 2D cyclotron frequency, $\mathcal{E}_c = e\mathcal{A} a_w \Omega_w / c$ the characteristic energy for the coupling between electrons and cavity photons, $a_w = \sqrt{\hbar/(m^* \Omega_w)}$ the characteristic oscillator length scale and $\mathcal{N}_e = \sum_i d_i^\dagger d_i$ the electron number operator. In equation (16), we use the dimensionless coupling g_{ij} between the electrons and the cavity modes defined by

$$g_{ij} = \frac{a_w}{2\hbar} \int d\mathbf{r} \left[\psi_i^*(\mathbf{r}) \left\{ (\hat{\mathbf{e}} \cdot \boldsymbol{\pi}) \psi_j(\mathbf{r}) \right\} + \left\{ (\hat{\mathbf{e}} \cdot \boldsymbol{\pi}) \psi_i(\mathbf{r}) \right\}^* \psi_j(\mathbf{r}) \right], \tag{17}$$

with $\hat{\mathbf{e}} \cdot \boldsymbol{\pi} = e_x \pi_x + e_y \pi_y$. The first and the second terms in equation (16) contribute, respectively, to the linear and nonlinear optical excitation energy spectra, which will be explored later.

In our theoretical consideration, we will formally consider all the higher-lying photonic modes, truncating the infinite matrix in order to retain enough modes to reach sufficient convergence. To obtain a convergent energy spectrum from the total Hamiltonian equation (1), all the resonant and anti-resonant terms in the photon creation and annihilation operators will be taken into account with arbitrary detuning. In the case of resonance, the condition of the vacuum Rabi frequency to the cyclotron frequency ratio larger than one implies that the higher photonic modes are coupled to the transition, and the diamagnetic A^2 term of the electron–photon coupling in equation (13) becomes dominant [28].

In the MES basis $\{|\mu)\}$, we can rewrite the electron–photon interaction Hamiltonian as

$$H_{e-EM} = \mathcal{E}_c \sum_{\mu\nu ij} |\mu)\langle\mu|\mathcal{V}^\dagger d_i^\dagger d_j \mathcal{V}|\nu\rangle(\nu| \, g_{ij} \left\{a + a^\dagger\right\} + \frac{\mathcal{E}_c^2}{\hbar \Omega_w} \sum_{\mu\nu j} |\mu)\langle\mu|\mathcal{V}^\dagger d_j^\dagger d_j \mathcal{V}|\nu\rangle(\nu|$$
$$\times \left\{ \left(a^\dagger a + \frac{1}{2} \right) + \frac{1}{2} \left(aa + a^\dagger a^\dagger \right) \right\}. \tag{18}$$

The energy spectrum of the total Hamiltonian involving both the electron–photon and electron–electron interactions has to be obtained from the many-body space of the interacting

electrons $\{|\mu)\}$ and the Fock space of photons $\{|M_{\rm ph}\rangle\}$, namely the uncoupled electron–photon many-body states (MBSs) $|\breve{\mu}\rangle = |\mu) \otimes |M_{\rm ph}\rangle$. Using the noninteracting electron–photon MBSs, performing diagonalization of the total Hamiltonian (1), the interacting electron–photon MBSs $|\breve{\mu})$ can be expressed as

$$|\breve{\mu}) = \sum_{\nu} \mathcal{W}_{\mu\nu} |\breve{\nu}\rangle. \tag{19}$$

It is important to note that in arriving at equation (19) we have performed truncations to a basis two times. The first one is when we only use the $N_{\rm SES}$ SESs to construct our Fock-space basis $\{|\mu\rangle\}$. The second is when we only use $N_{\rm MES}$ Coulomb interacting states $|\mu)$ and $N_{\rm EM}$ photon states to construct the joint photon–electron many-body basis $\{|\mu) \otimes |M_{\rm ph}\rangle\}$. A third truncation is likely to be needed if one needs to apply operations involving $\mathcal{W}$ many times, for example in time-dependent calculations [31]. However, in this paper, only static properties are calculated such as the energy spectrum and charge densities of the many-body eigenstates. Therefore, a third truncation is not necessary.

The electron charge density operator $Q(\mathbf{r})$ in the electron–photon coupled system in the second quantized form is

$$Q(\mathbf{r}) = -e \sum_{i,j} \psi_i^*(\mathbf{r}) \psi_j(\mathbf{r}) d_i^\dagger d_j. \tag{20}$$

By taking trace of the operators in the coupled MBS space $\{|\breve{\mu})\}$, we obtain the correlated many-body charge distribution $\langle Q(\mathbf{r})\rangle$ for the electrons in the nanostructure interacting with the photon field

$$\langle Q(\mathbf{r})\rangle = {\rm Tr}\left\{\rho(t) \mathcal{W}^\dagger Q(\mathbf{r}) \mathcal{W}\right\}. \tag{21}$$

It should be mentioned that the total density operator $\rho(t)$ contains information on the interacting many-electron system and the monochromatic photon modes as well.

Below, we demonstrate our numerical results displaying tunable dynamical interplay features between the interacting electrons and the quantized photon field with either the x- or the y-polarized electric components in an external magnetic field. We mention in passing that in the construction of the JC model, we assume only two electron states to be active in the system. However, when we take into account a realistic geometry, a sufficient number of electron states will be used to guarantee numerical convergence.

3. Results and discussion

In order to explore the dynamical features of an electronic system coupled to a single-mode quantum photon field, a simple TLS model is often employed [32–34]. The energy spectrum of the TLS can be used to employ the JC model [14]. Although the JC model has been applied beyond the RWA, a rigorous analysis of the validity of the JC model in a realistic system remains unexplored. It is thus useful to consider an electronic nanostructure coupled to cavity photons taking into account realistic geometrical effects, by performing numerical computation beyond the JC model for comparison.

We assume that the electric nanostructure is fabricated by GaAs-based semiconducting materials with the electron effective mass $m^* = 0.067 m_{\rm e}$ and the background relative dielectric constant $\kappa = 12.4$. The electronic nanostructure is modeled as an infinite square potential well of

length $L_x = 300\,\text{nm}$ along the x-axis and transversely constricted by split-gates with a parabolic confinement strength $\hbar\Omega_0 = 1.0\,\text{meV}$ along the y-axis. A uniform and static magnetic field $B = 0.1\,\text{T}$ is applied along the z-axis. In order to obtain the energy spectra of the closed electron–photon system, we have used $N_{\text{MES}} = 200$ electron states and $N_{\text{EM}} = 20$ photon states. The two-electron MESs have been computed with $N_{\text{SES}} = 50$ and the SESs with $N_{\text{SES}} = N_{\text{MES}}$. No calculations for three or more electrons are needed in this paper.

The MBS energy spectra of the electron–photon states are shown in figures 1 and 2 for the case of x- and y-polarizations, respectively, corresponding to the TE_{011} and TE_{101} modes. The single-photon energy is $\hbar\omega = 0.4\,\text{meV}$; hence, the M_{ph} photon states with no electrons have the energy $E_{\text{ph}} = M_{\text{ph}}\hbar\omega$. The horizontal axis $\mathcal{E}_{\text{c}}$ denotes the strength of coupling between the electrons and the photons. In the absence of the electron–photon coupling $\mathcal{E}_{\text{c}} = 0$, both the cases of x- and y-polarizations manifest the same energy spectra.

In the weak electron–photon coupling regime $\mathcal{E}_{\text{c}} \leqslant 0.1\hbar\omega$, the energy spectra of a linear approximation neglecting the A^2 term (red) are only slightly shifted from the full numerical results including the A^2 term (blue), and the pure photon states (green) retain the same energy. However, the linear approximation neglecting the A^2 term becomes inaccurate when the coupling strength $\mathcal{E}_{\text{c}}$ is comparable to the driving photon energy $\hbar\omega$ and the characteristic energy level spacing of the electronic system.

Our full numerical results clearly show that the lowest two many-body energy states at around $E = 0.56$ and $0.75\,\text{meV}$ are not sensitive to the polarization of the quantized electromagnetic field. However, the higher MBSs may be sensitive to the polarization of the photon field. Moreover, comparing figures 1 and 2, we see that the energy dispersion is much more sensitive to the x-polarized photon field than that of y-polarization. This is because the single-photon energy $\hbar\omega$ is comparable to the characteristic energy of the lowest states in the nanostructure for electron motion in the x-direction. In other words, it is caused by the anisotropy of the selected geometry. In addition, for the case of x-polarization the two states at around MBS energy $E_{\text{MBS}} \approx 1.0\,\text{meV}$ cross at $\mathcal{E}_{\text{c}} \approx 0.16\,\text{meV}$, but not in the case of y-polarization.

We will now analyze the validity of the TLS approximation, as well as the even simpler JC model. The JC model is built from a TLS relying upon the assumptions of near resonance and weak coupling between the two systems that is described by the following Hamiltonian in the second quantized form:

$$H_{\text{JC}} = \frac{1}{2}\Delta E_{ij}\sigma_z + \hbar\omega a^\dagger a + \mathcal{E}_{\text{JC}}\left(\sigma_+ + \sigma_-\right)\left(a + a^\dagger\right), \tag{22}$$

where $\Delta E_{ij} = E_j - E_i$ denotes the energy difference between the electron states $|i\rangle$ and $|j\rangle$, which have been chosen as the relevant states for the TLS approximation. The ladder operators appropriate for a two-level approximation $\sigma_\pm$ are defined by $\sigma_\pm = \frac{1}{2}(\sigma_x \pm \text{i}\sigma_y)$, where $\sigma_{x,y,z}$ are the Pauli matrices. Note that the energies of states $|i\rangle$ and $|j\rangle$ have been shifted to make them symmetric around the zero energy.

The counter-rotating terms $\sigma_+ a^\dagger$ and $\sigma_- a$ in equation (22) are usually omitted by taking the RWA to get an exactly solvable model. However, for our comparison we will keep the counter-rotating terms and solve equation (22) numerically using the Fock-space basis $\{|k\rangle \otimes |M_{\text{ph}}\rangle\}$, where $k \in \{i, j\}$. Comparison of the JC model with and without the counter-rotating terms has been investigated [32–34]; however, it should be reexamined and compared with a system where realistic effects are included, such as those stemming from the nontrivial geometry of the nanostructure and an external magnetic field.

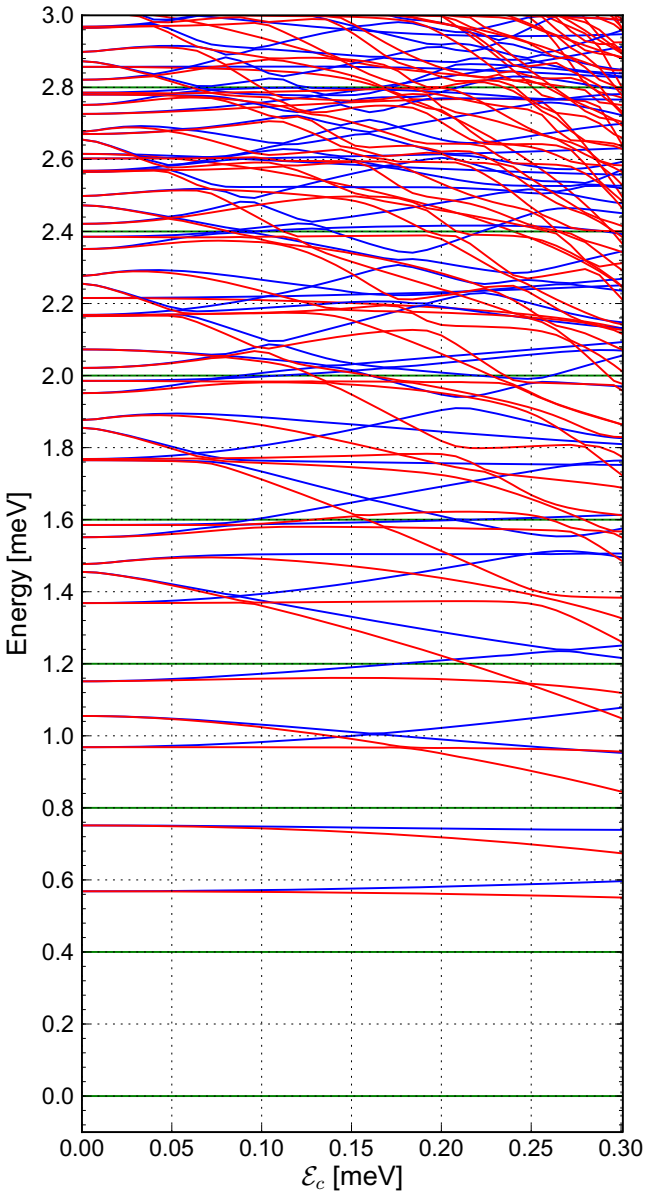

Figure 1. The many-body energy spectra for the interacting-electron and quantized-photon modes versus the electron–photon coupling strength $\mathcal{E}_c$ for the case of the TE_{011} mode (the electric component with x-polarization). Shown are the pure photon states with no electron (green), the MBSs without the A^2 term (red) and the MBSs including the A^2 term (blue). The majority of the states contain a single electron. Two-electron states are present for energy >2.0 meV. Other parameters are $B = 0.1$ T, $\hbar\Omega_0 = 1.0$ meV and $\hbar\omega = 0.4$ meV.

For a TLS with one electron, zero magnetic field and ignoring the $\mathcal{E}_c^2$ term in equation (18), the total Hamiltonian in equation (1) reduces to a JC-like Hamiltonian with a coupling strength $\mathcal{E}_{JC}$ associated with $\mathcal{E}_c$ according to

$$\mathcal{E}_{JC} = |g_{ij}|\mathcal{E}_c, \tag{23}$$

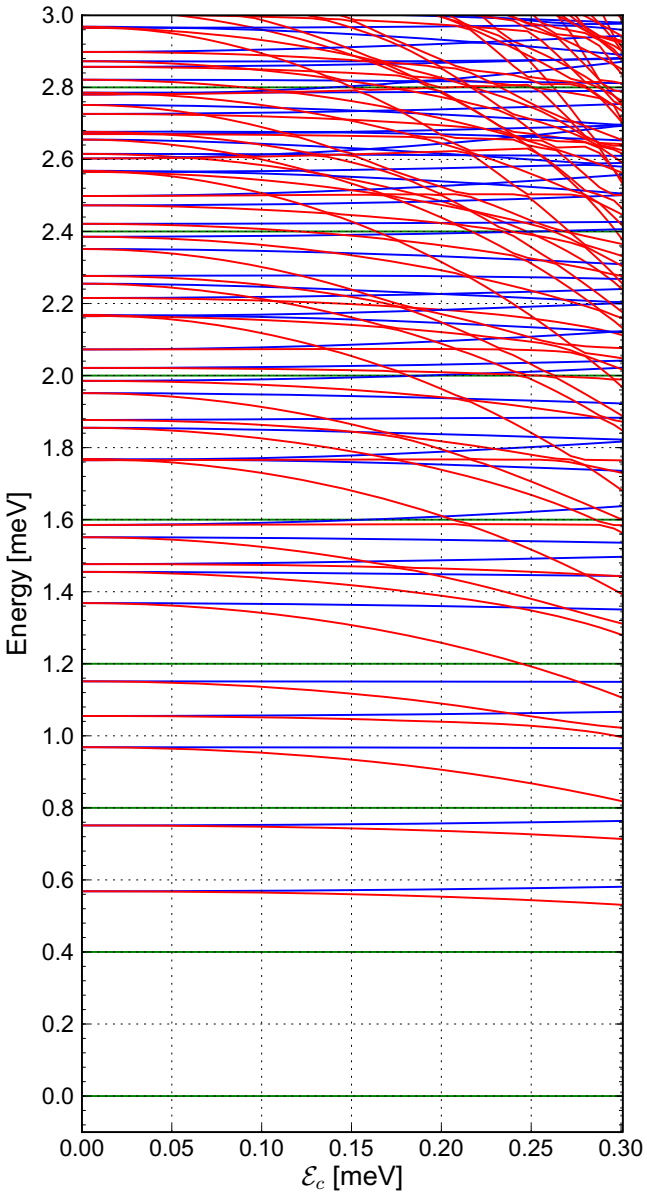

Figure 2. The many-body energy spectra for the interacting-electron and quantized-photon modes versus the electron–photon coupling strength $\mathcal{E}_c$ for the case of the TE_{101} mode (the electric component with y-polarization). Shown are pure photon states with no electron (green), the MBSs without the A^2 term (red) and the MBSs including the A^2 term (blue). The majority of the states contain a single electron. Two-electron states are present for energy >2.0 meV. Other parameters are $B = 0.1$ T, $\hbar\Omega_0 = 1.0$ meV and $\hbar\omega = 0.4$ meV.

in which the dimensionless coupling constant g_{ij} can be calculated using equation (17). For a nonzero magnetic field, equation (23) is not exact; however, as will be shown later, a low magnetic field $B = 0.1$ T has minimal effects.

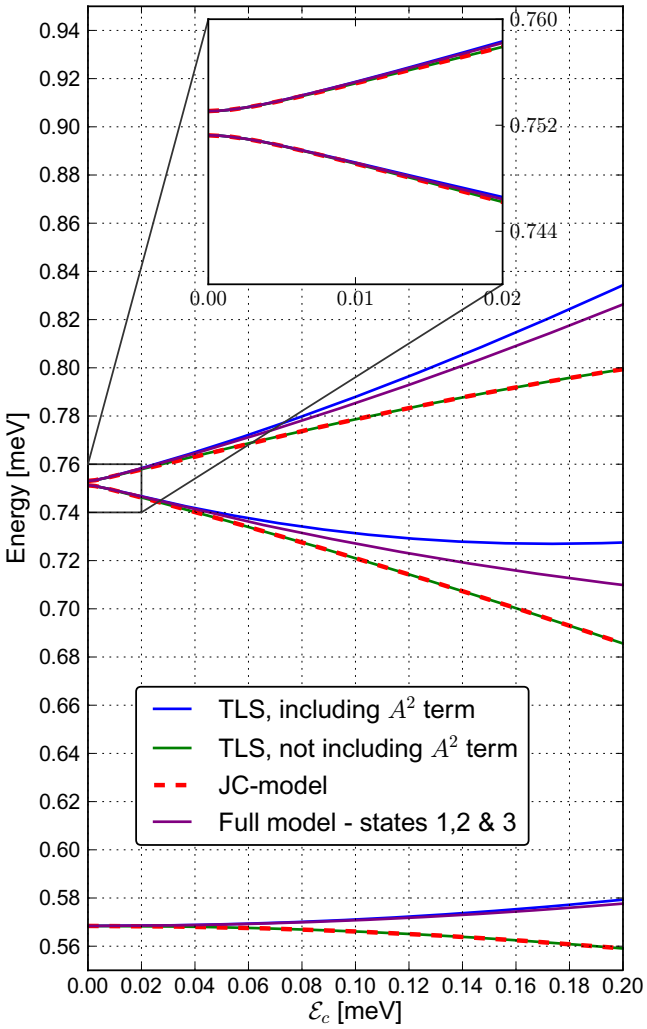

Figure 3. Comparison of the many-body energy spectra versus the coupling strength $\mathcal{E}_c$ for the case of TE_{011} mode (x-polarization). The energy spectra are obtained by the TLS model with (blue) and without (green) the A^2 term and the JC model (red dashed). The TLS model results are compared with the full numerical calculation results for the lowest active levels 1, 2 and 3 (purple). Other parameters are $B = 0.1\,\mathrm{T}$, $\hbar\Omega_0 = 1.0\,\mathrm{meV}$, $|g_{12}| = 0.701$ and $\hbar\omega = 0.185\,\mathrm{meV}$. The inset shows the validity of the JC model in the weak coupling limit.

Below we will assume that the detuning δ is 1% of the energy spacing of the two active states ΔE_{ij} giving the single-photon energy $\hbar\omega = 1.01\Delta E_{ij}$. To label energy levels the notation E_k^M is used. It refers to the energy of the state $|k\rangle \otimes |M_{\mathrm{ph}}\rangle$ for $\mathcal{E}_c = 0$.

Figure 3 shows the x-polarization many-body energy spectra as a function of the electron–photon coupling strength for the different models. We consider the lowest states $|1\rangle$ and $|2\rangle$ as the relevant states for the TLS. In the zero coupling limit $\mathcal{E}_c = 0$, the ground state energy $E_1 = E_1^0 \simeq 0.568\,\mathrm{meV}$ and the energy of the first excited state is $E_2 = E_2^0 \simeq 0.751\,\mathrm{meV}$,

so that the energy level spacing is $\Delta E_{12} = 0.183\,\text{meV}$. The detuning is small compared to the typical energy difference of the electron states so the third state is associated with one-photon absorption from state $|1\rangle$ with energy $E_3 = E_1^1 = E_1^0 + \hbar\omega = 0.753\,\text{meV}$. As expected, the JC results almost coincide with our TLS results not including the A^2 term. The difference (not visible in figure 3) between the two curves is due to the effects of the external magnetic field. When the A^2 term is included, the energy spectrum manifests a blue-shift, and the energy-level correction δE may be larger than 0.02 meV in the strong-coupling regime, or $\delta E/\Delta E > 10\%$. A weaker red-shift correction is observed when the higher MBSs are involved in the electron–photon coupling.

In the weak coupling regime $\mathcal{E}_c < 0.1\hbar\omega \simeq 0.02\,\text{meV}$, the JC model is approximately valid. When the coupling strength is increased to $\mathcal{E}_c \simeq \hbar\omega \approx 0.2\,\text{meV}$, the ground state energy calculated by the TLS model is still valid. However, the energy of the excited states becomes inaccurate, indicating that the simplified TLS model is no longer a good approximation in the strong coupling regime even though the diamagnetic vector potential A^2 is included. When the coupling strength $\mathcal{E}_c$ is increased, both the JC model and the TLS without the A^2 term predict a decreasing ground state; however, by including the A^2 term within the TLS model the energy increases, in better agreement with our full numerical calculation.

In figure 4, we compare the many-body energy spectra as a function of the electron–photon coupling strength $\mathcal{E}_c$ when the electronic system is embedded in a TE_{101} mode (y-polarization). Attributed to selection rules of the transverse parabolic confinement, we select the active states $|1\rangle$ and $|5\rangle$ to compare with the TLS approximation. In the zero coupling limit $\mathcal{E}_c = 0$, we consider the ground state energy $E_1^0 \simeq 0.568\,\text{meV}$ and the excited state energy $E_5^0 \simeq 1.585\,\text{meV}$ so that the energy level spacing $\Delta E_{15} = 1.017\,\text{meV}$. In addition, we assume the detuning $\delta_{15} = 0.01 \times \Delta E_{15}$ such that the single-photon energy $\hbar\omega = \Delta E_{15} + \delta_{15} = 1.027\,\text{meV}$. Moreover, we see that the state associated with a ground state electron absorbing one photon is around $E_1^1 = E_1^0 + \hbar\omega = 1.596\,\text{meV}$.

Figure 4 displays energy spectra calculated using the different models. As with the x-polarization, the energy spectrum obtained by the JC model almost coincides with the TLS result without the A^2 term. The difference (not visible in figure 4) is due to the effects of the external magnetic field. When the A^2 term is included, the energy spectrum is blue-shifted in the strong coupling regime. When higher MBSs are involved in the electron–photon coupling (full model), there is good agreement with the TLS including the A^2 term until inactive states (not included in the two-level approximation) start to have an influence, such as the energy crossing at $\mathcal{E}_c \simeq 0.13\,\text{meV}$ and anti-crossing at $\mathcal{E}_c \simeq 0.17\,\text{meV}$ shown in figure 4. In the weak coupling regime $\mathcal{E}_c < 0.1\hbar\omega \simeq 0.1\,\text{meV}$, the JC model is approximately valid. The ultrastrong coupling regime $\mathcal{E}_c > \hbar\omega \simeq 1.0\,\text{meV}$ is not shown in this figure.

The effects of the photon field on the charge distribution is illustrated in figure 5, where the charge distribution $\langle Q(\mathbf{r})\rangle$ of the third MBS is plotted for x-polarization for $\mathcal{E}_c = 0,\ 0.2,\ 0.3$ and 0.4 meV. There is an energy crossing between the third and fourth states at $\mathcal{E}_c \simeq 0.16$ (see figure 1) so it is important to note that for $\mathcal{E}_c > 0.16$, the third state refers to the fourth state counting from the bottom in figure 1. In figure 5(a), the energy of the MBS is $E_0^1 \simeq 0.96\,\text{meV}$. There is no coupling between the photons and electrons so the charge density is identical to that of the ground state labeled by the energy E_0^0. For $\mathcal{E}_c = 0.2\,\text{meV} = \hbar\omega/2$, the charge distribution is stretched in the x-direction. This trend continues with increasing coupling strength. For $\mathcal{E}_c = 0.3\,\text{meV}$ the charge distribution starts to separate into two peaks and at $\mathcal{E}_c = 0.4\,\text{meV}$ the two peaks are completely separated. In other words, in the ultrastrong coupling regime $\mathcal{E}_c = \hbar\omega$,

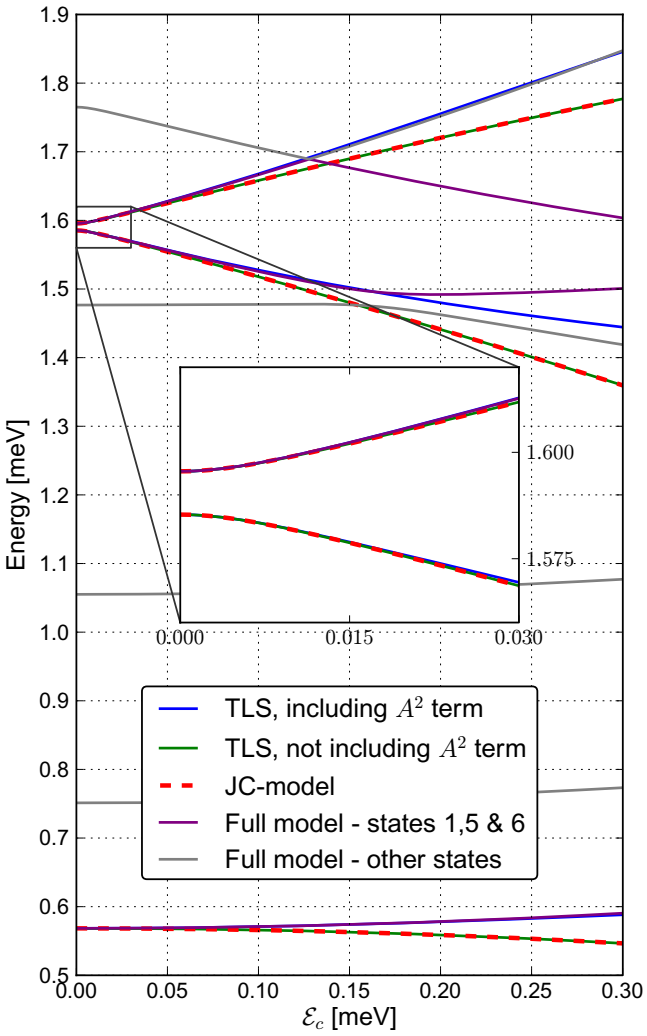

Figure 4. Comparison of the many-body energy spectra versus the coupling strength $\mathcal{E}_c$ for the case of the TE_{101} mode (y-polarization). These energy states are obtained by the TLS model including the A^2 term (blue), not including the A^2 term (green) and the JC approximation without magnetic field (red dashed). The TLS model results are compared with the full numerical calculation for the compared lowest active levels 1, 5 and 6 (purple) as well as inactive levels (gray). Other parameters are $B = 0.1\,\mathrm{T}$, $\hbar\Omega_0 = 1.0\,\mathrm{meV}$, $|g_{1,5}| = 0.290$ and $\hbar\omega = 1.027\,\mathrm{meV}$. The inset shows the validity of the JC model in the weak coupling limit.

a clear dipole-like charge distribution profile is observed. For the y-polarization, not shown here, the polarization of the charge is much smaller due to the large value of the confinement energy $\hbar\Omega_0 = 1.0\,\mathrm{meV}$ compared to the photon energy $\hbar\omega = 0.4\,\mathrm{meV}$. The system is anisotropic at the energy scale we employ here.

To summarize this section, we remind the reader that the JC model exhibits energy spectrum with some levels decreasing when the electron–photon coupling is increased [32, 33].

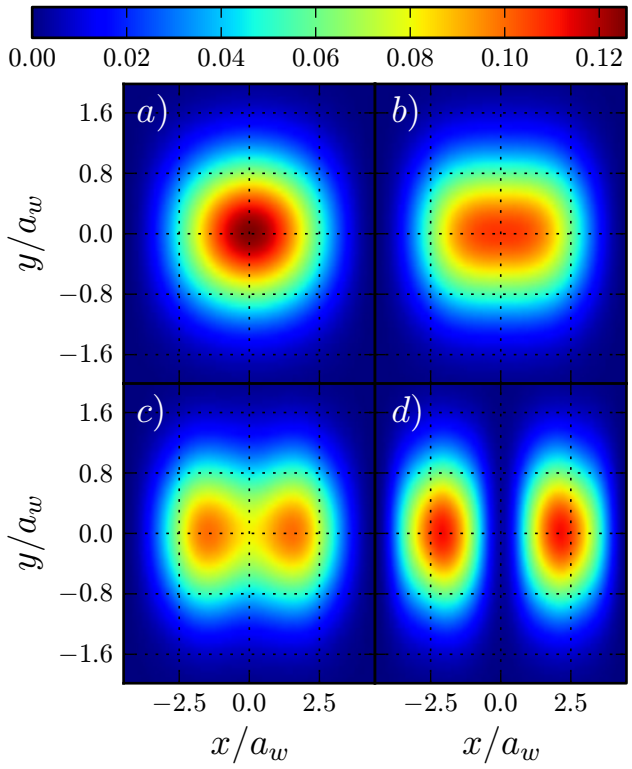

Figure 5. Charge distribution (in units of $-e$) of the third many-body state (see text for definition) in the case of x-polarization with electron–photon coupling strength $\mathcal{E}_c =$ (a) 0.0, (b) 0.2, (c) 0.3 and (d) 0.4 meV. The other parameters are the same with figure 1: $B = 0.1$ T, $\hbar\Omega_0 = 1.0$ meV and $\hbar\omega = 0.4$ meV.

The energies may be negative if the electron–photon coupling is very strong [32]. Comparing with the full numerical calculation, it is thus unambiguous that the diamagnetic A^2 contribution as well as higher energy electron states have to be included in the ultrastrong coupling regime. We have done a simple literature search for 'ultrastrong' and 'circuit-QED'. One has to keep in mind that authors have not always used the same definition for strong or ultrastrong, but none found in our search results either included the A^2 term in their model or went beyond the two-level approximation.

4. Concluding remarks

We have performed a numerical calculation of a microscopic model describing a hybrid structure consisting of an electronic nanostructure embedded in a cavity resonator. We have demonstrated strong coupling features of Coulomb interacting electrons and photons in a nanostructure embedded in a cavity resonator in an external magnetic field. The two-dimensional electronic nanostructure is parabolically confined in the y-direction and hard-wall confined in the x-direction that is embedded in a rectangular photon cavity with a TE-mode electromagnetic field that may be either x- or y-polarized. We have found that the many-body energy spectrum is more sensitive to the photon field with x-polarized electric component than that with y-polarization for the selected geometry. The system is anisotropic in the energy range explored.

We have established that the diamagnetic A^2 term in the Hamiltonian may provide a blue-shift correction to the energy spectrum. However, when higher many-body states are included beyond a two-level approximation, the results of the full numerical calculation exhibit a smaller red-shift correction. This implies that the two lowest levels become more stable when higher energy levels are included in the electron–photon coupled system. When the A^2 term is not included, the energy spectrum decreases when the coupling strength is increased, but the opposite trend is found when the A^2 term is included in the calculation.

The widely employed TLS approximation has been reexamined using the results of our full numerical calculation model. Qualitative difference in the energy spectrum between the JC model and the full numerical calculation is found in the strong-coupling regime. The JC model includes no information about the charge distribution of the system. A strong cavity photon field can cause a large polarization of the charge distribution, an effect seen in figure 5. The reason for the high number of SESs needed in our full calculation is exactly this large polarizing effect of the photon field. The QED modeling of a circuit element on the nanoscale in the ultrastrong coupling regime requires approximations beyond the JC model or more general two-level models.

In summary, we have presented a model adequate for accurate numerical calculation of the coupled electron–photon energy spectrum that is essential and will be utilized to explore the time-dependent transport of electrons through a photon cavity in a forthcoming publication [31].

Acknowledgments

This work was supported by the Icelandic Research and Instruments Funds, the Research Fund of the University of Iceland. CST is grateful for support from the National Science Council, Taiwan, under grant numbers NSC97-2112-M-239-003-MY3 and NSC100-2112-M-239-001-MY3. HSG acknowledges support from the National Science Council, Taiwan, under grant numbers 97-2112-M-002-012-MY3 and 100-2112-M-002-003-MY3, the Frontier and Innovative Research Program of the National Taiwan University under grant numbers 99R80869 and 99R80871 and the focus group program of the National Center for Theoretical Sciences, Taiwan.

References

[1] Heinrich G, Harris J G E and Marquardt F 2010 *Phys. Rev.* A **81** 011801
[2] Rabl P 2011 *Phys. Rev. Lett.* **107** 063601
[3] Liu C, Dutton Z, Behroozi C H and Hau L V 2001 *Nature* **409** 490
[4] Golubeva T, Golubev Yu, Mishina O, Bramati A, Laurat J and Giacobino E 2011 *Phys. Rev.* A **83** 053810
[5] Yoshie T, Scherer A, Hendrickson J, Khitrova G, Gibbs H M, Rupper G, Ell C, Shchekin O B and Deppe D G 2004 *Nature* **432** 200
[6] Peter E, Senellart P, Martrou D, Lemaítre A, Hours J, Gérard J M and Bloch J 2005 *Phys. Rev. Lett.* **95** 067401
[7] Hennessy K, Badolato A, Winger M, Gerace D, Atatüre M, Gulde S, Fält S, Hu E L and Imamoğlu A 2007 *Nature* **445** 896
[8] Press D, Götzinger S, Reitzenstein S, Hofmann C, Löffler A, Kamp M, Forchel A and Yamamoto Y 2007 *Phys. Rev. Lett.* **98** 117402
[9] Wallraff A, Schuster D I, Blais A, Frunzio L, Huang R-S, Majer J, Kumar S, Girvin S M and Schoelkopf R J 2004 *Nature* **431** 162
[10] Niemczyk T *et al* 2010 *Nat. Phys.* **6** 772

[11] Hoffmann E *et al* 2010 *Appl. Phys. Lett.* **97** 222508
[12] Delbecq M R, Schmitt V, Parmentier F D, Roch N, Viennot J J, Fève G, Huard B, Mora C, Cottet A and Kontos T 2011 *Phys. Rev. Lett.* **107** 256804
[13] Frey T, Leek P J, Beck M, Blais A, Ihn T, Ensslin K and Wallraff A 2011 *Phys. Rev. Lett.* accepted (arXiv:1108.5378)
[14] Jaynes E T and Cummings F W 1963 *Proc. IEEE* **51** 89
[15] Raimond J M, Brune M and Haroche S 2001 *Rev. Mod. Phys.* **73** 565
[16] Haroche S and Raymond J-M 2006 *Exploring the Quantum* (New York: Oxford University Press)
[17] Shore B W and Knight P L 1993 *J. Mod. Opt.* **40** 1195
[18] Wang L, Puri R R and Eberly J H 1992 *Phys. Rev.* A **46** 7192
[19] Wu Y 1996 *Phys. Rev.* A **54** 4534
[20] Helm M 2000 *Intersubband Transitions in Quantum Wells: Physics and Device Applications I* ed H C Liu and F Capasso (New York: Academic) pp 1−99
[21] Gabbay A, Reno J, Wendt J R, Gin A, Wanke M C, Sinclair M B, Shaner E and Brener I 2011 *Appl. Phys. Lett.* **98** 203103
[22] Ciuti C, Bastard G and Carusotto I 2005 *Phys. Rev.* B **72** 115303
[23] Devoret M, Girvin S and Schoelkopf R 2007 *Ann. Phys.* **16** 767
[24] Abdumalikov A A, Astafiev O, Nakamura Y, Pashkin Y A and Tsai J 2008 *Phys. Rev.* B **78** 180502
[25] De Zela F, Solano E and Gago A 1997 *Opt. Commun.* **142** 106
[26] Sornborger A T, Cleland A N and Geller M R 2004 *Phys. Rev.* B **70** 052315
[27] Irish E K 2007 *Phys. Rev. Lett.* **99** 173601
[28] Hagenmüller D, Liberato S D and Ciuti C 2010 *Phys. Rev.* B **81** 235303
[29] Yannouleas C and Landman U 2007 *Rep. Prog. Phys.* **70** 2067
[30] Gudmundsson V, Gainar C, Tang C-S, Moldoveanu V and Manolecu A 2009 *New J. Phys.* **11** 113007
[31] Gudmundsson V, Jonasson O, Tang C-S, Goan H-S and Manolescu A 2011 *Phys. Rev.* B submitted (arXiv:1109.4728)
[32] Feranchuk I D, Komarov L I and Ulyanenkov A P 1996 *J. Phys. A: Math. Gen.* **29** 4035
[33] Chen Q-H, Liu T, Zhang Y-Y and Wang K-L 2011 *Europhys. Lett.* **96** 14003
[34] Zhang Y, Chen G, Yu L, Liang Q, Liang J-Q and Jia S 2011 *Phys. Rev.* A **83** 065802